

Automated Seismic Source Characterisation Using Deep Graph Neural Networks

M. P. A. van den Ende¹, J.-P. Ampuero¹

¹Université Côte d'Azur, IRD, CNRS, Observatoire de la Côte d'Azur, Géoazur, France

Key Points:

- We propose a deep learning approach for automated earthquake location and magnitude estimation based on Graph Neural Network theory
- This new approach processes multi-station waveforms and incorporates station locations explicitly
- Including station locations improves the accuracy of epicentre estimation compared to models that are location-agnostic

Corresponding author: M. P. A. van den Ende, martijn.vandenende@geoazur.unice.fr

Abstract

Most seismological analysis methods require knowledge of the geographic location of the stations comprising a seismic network. However, common machine learning tools used in seismology do not account for this spatial information, and so there is an underutilised potential for improving the performance of machine learning models. In this work, we propose a Graph Neural Network (GNN) approach that explicitly incorporates and leverages spatial information for the task of seismic source characterisation (specifically, location and magnitude estimation), based on multi-station waveform recordings. Even using a modestly-sized GNN, we achieve model prediction accuracy that outperforms methods that are agnostic to station locations. Moreover, the proposed method is flexible to the number of seismic stations included in the analysis, and is invariant to the order in which the stations are arranged, which opens up new applications in the automation of seismological tasks and in earthquake early warning systems.

Plain language summary

To determine the location and size of earthquakes, seismologists use the geographic locations of the seismic stations that record the ground shaking in their data analysis workflow. By taking the distance between stations and the relative timing of the onset of the shaking, the origin of the seismic waves can be accurately reconstructed. In recent years, machine learning (a subfield of artificial intelligence) has shown great potential to automate seismological tasks, such as earthquake source localisation. Most machine learning methods do not take into consideration the geographic locations of the seismic stations, and so the usefulness of these methods could still be improved by providing the locations at which the data was recorded. In this work, we propose a method that accounts for geographic locations of the seismic stations, and we show that this improves the machine learning predictions.

1 Introduction

Seismic source characterisation is a primary task in earthquake seismology, and involves the estimation of the epicentral location, hypocentral depth, and moment of the seismic source. Particularly for the purposes of earthquake early warning, emergency response and timely information dissemination, an estimate of the seismic source characteristics needs to be produced rapidly, preferably without the intervention of an analyst.

43 One computational tool that satisfies these requirements is machine learning, making it
44 a potential candidate to address the challenge of rapid seismic source characterisation.

45 Recently, attempts have been made to apply machine learning to seismic source
46 characterisation (Käuffl et al., 2014; Perol et al., 2018; Lomax et al., 2019; Kriegerowski
47 et al., 2019; Mousavi & Beroza, 2020b,a). In the ConvNetQuake approach of Perol et
48 al. (2018), a convolutional neural network was adopted to distinguish between noise and
49 earthquake waveforms, and to determine the regional earthquake cluster from which each
50 event originated. This method was extended by Lomax et al. (2019) to global seismic-
51 ity. Mousavi & Beroza (2020b) employed a combined convolutional-recurrent neural net-
52 work to estimate earthquake magnitudes. It is noteworthy that these methods only ac-
53 cept single-station waveforms as an input, which goes against the common intuition that
54 at least three seismic stations are required to triangulate and locate a seismic source. One
55 possible explanation for the performance of these methods is that they rely on waveform
56 similarity (Perol et al., 2018) and differences in phase arrival times (Mousavi & Beroza,
57 2020b). Unfortunately, since the parametrisation through high-dimensional machine learn-
58 ing methods does not carry a clear physical meaning, this hypothesis is not easily tested.

59 Alternatively, a multi-station approach would take as input for each earthquake all
60 the waveforms recorded by the seismic network. One compelling argument in favour of
61 single-station approaches is that for each earthquake there are as many training sam-
62 ples as there are stations, whereas in the multi-station approach there is only one train-
63 ing sample per earthquake (the concatenated waveforms from the whole network). Since
64 the performance of a deep learning model tends to benefit from larger volumes of data
65 available for training, the model predictions may not improve when combining multiple
66 station data into a single training sample. Second, micro-earthquakes are usually not recorded
67 on multiple seismic stations if the seismic network is sparse, warranting further devel-
68 opment of single-station methods. Lastly, concatenating data from multiple stations in
69 a meaningful way is non-trivial. If the seismic network has a Euclidean structure, i.e. if
70 it is arranged in a regular pattern like for uniformly-spaced seismic arrays or fibre-optic
71 distributed acoustic sensing, the data can be naturally arranged into e.g. a 2D image,
72 where the distance between each pixel is representative of the spatial sampling distance.
73 Unfortunately, most seismic networks are not arranged in a regular structure, so that
74 the geometry of the network needs to be learned implicitly, as was attempted by Kriegerowski
75 et al. (2019). Even though this approach yielded acceptable hypocentre location estimates,

76 it remains an open question whether better results could be achieved when the non-Euclidean
77 nature of the seismic network is better accounted for. Moreover, the seismic stations com-
78 prising the network may not be continuously operational over the period of interest (due
79 to (de)commissioning, maintenance, or temporary campaigning strategies), leading to
80 gaps in the fixed Euclidean data structure. Rather, seismic networks are better repre-
81 sented by a time-varying *graph* structure.

82 The deep learning tools most commonly used in seismology, convolutional neural
83 networks (CNNs) and multi-layer perceptrons (MLPs) (see also Supplementary Text S1;
84 Rosenblatt, 1957; Fukushima, 1980; Rumelhart et al., 1986; LeCun et al., 2015; Schramowski
85 et al., 2020), are well suited to Euclidean data structures, but are not optimal for graph
86 data structures. One important characteristic of graphs is that they are not defined by
87 the ordering or positioning of the data, but only by the relations between data. As such,
88 valid operations on a graph need to be invariant to the data order. This is not gener-
89 ally the case for CNNs, which exploit ordering as a proxy for spatial distance, nor for
90 MLPs, which rely on the constant structure of the input features. Fortunately, much progress
91 has been made in the field of *Graph Neural Networks* (GNNs; Gori et al., 2005; Scarselli
92 et al., 2009; Zhou et al., 2019), providing a robust framework for analysing non-Euclidean
93 data using existing deep learning tools.

94 In this contribution, we will demonstrate how GNNs can be applied to seismic source
95 characterisation using data from multiple seismic stations simultaneously. The method
96 does not require a fixed seismic network configuration, and so the number of stations to
97 be included in each sample is allowed to vary over time. Moreover, the stations do not
98 need to be ordered geographically or as a function of distance from the seismic source.
99 This makes the proposed method suitable for earthquake early warning and disaster re-
100 sponse applications, in which the number and location of stations on which a given event
101 is recorded is not known a-priori.

102 2 Methods

103 2.1 Basic Concepts of Graph Neural Networks

104 Over the past several years, numerous deep learning techniques have been proposed
105 that allow for the analysis of non-Euclidean data structures (Bronstein et al., 2017; Zhou
106 et al., 2019), which has found applications in point cloud data (Qi et al., 2017; Wang et

107 al., 2019), curved manifolds (Monti et al., 2017), and N -body classical mechanics (Sanchez-
108 Gonzalez et al., 2019), among many others. As a subclass of non-Euclidean objects, graphs
109 highlight relations between objects, typically represented as nodes connected by edges.
110 Commonly studied examples of graph-representable objects include social networks (Hamil-
111 ton et al., 2017), molecules (Duvenaud et al., 2015), and urban infrastructures (Cui et
112 al., 2019). Owing to the lack of spatial ordering of graph structures, mathematical op-
113 erations performed on graphs need to be invariant to the order in which the operations
114 are executed. Moreover, nodes and relations between them (i.e. the edges) may not be
115 fixed, and so the graph operations need to generalise to an arbitrary number of nodes
116 and/or edges (and potentially the number of graphs) at any given moment. In essence,
117 suitable graph operations are those that can be applied to the elements of a *set* of un-
118 known cardinality. These can be simple mathematical operations such as taking the mean,
119 maximum, or sum of the set, or they can involve more expressive aggregation (Battaglia
120 et al., 2018) and message passing (Gilmer et al., 2017) operations.

121 To make the above statement more concrete, we represent a seismic network by an
122 edgeless graph in which each seismic station is a node. In the context of seismic source
123 characterisation, information travels from the seismic source to each individual receiver
124 station independently of the relative positions between the stations. Since no informa-
125 tion is transmitted from one station to another, it is not intuitive to include e.g. the rel-
126 ative distance between two stations. While local site amplifications could play an im-
127 portant role in the seismic source characterisation process, such information should be
128 encoded in the absolute location of each station rather than the relative location. Hence,
129 for the task of seismic source characterisation, the relations between individual stations
130 are not physically meaningful, and so we do not include edges connecting the nodes in
131 the analysis, reducing the graph to an unordered set. While a graph with no edges may
132 seem ludicrous, the existence of edges is not a requirement for defining a graph, and ba-
133 sic architectural principles (e.g. Battaglia et al., 2018) still apply. Naturally, in cases where
134 the relation between stations is relevant, for example in seismic array beamforming (which
135 relies on relative locations and arrival times), edge information should be included. Each
136 node in our graph carries two attributes: a three-component seismic waveform time-series,
137 and a geographic location. The graph itself carries four attributes: the latitude, longi-
138 tude, depth, and magnitude of the seismic source. Through suitable processing and ag-

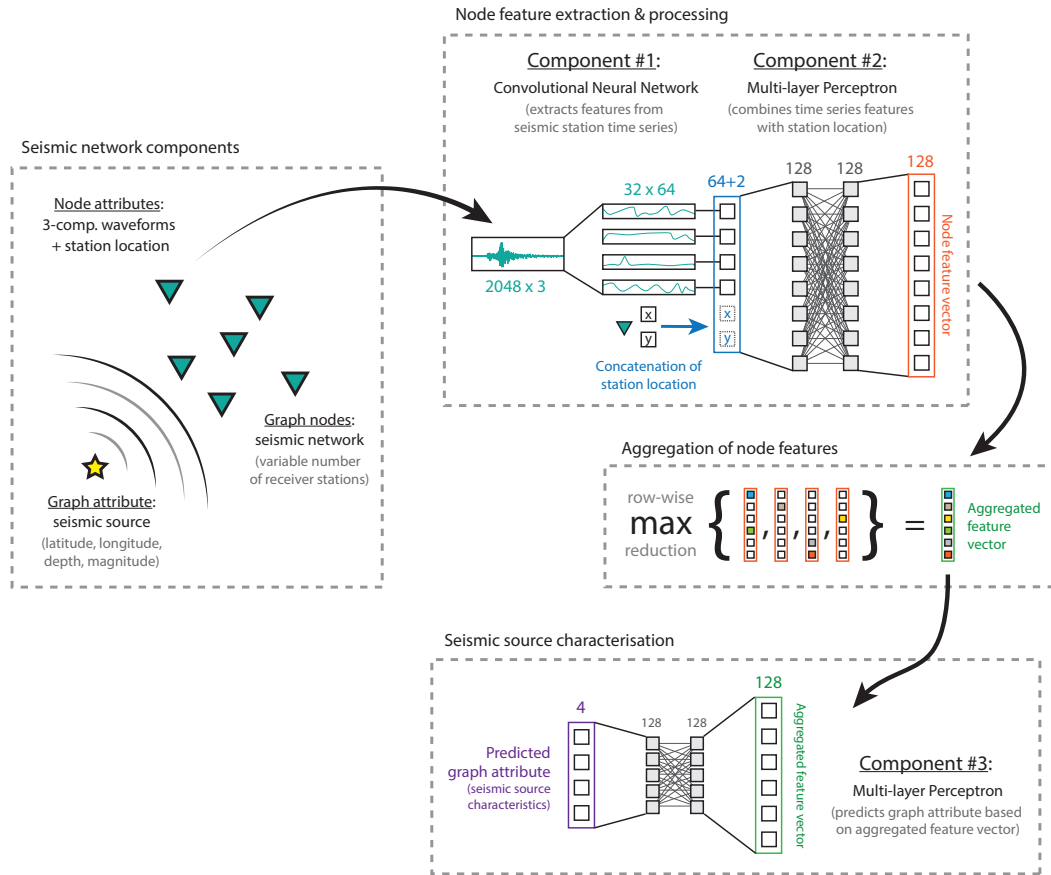


Figure 1. Synoptic overview of the adopted model architecture. The three-component waveforms from a receiver station are fed into a CNN, after which the extracted features are combined with the station’s geographic location and further processed by an MLP. The resulting node feature vector of all the stations are aggregated, and this aggregated feature vector is passed through a second MLP that predicts the seismic source characteristics.

139 aggregation of the node attributes, the objective for the GNN is to predict the graph at-
 140 tributes.

141 2.2 Model architecture

142 The model architecture employed in this work consists of three components that
 143 operate sequentially – see Fig. 1 and Supplementary Text S2 for details (Tompson et al.,
 144 2015; Saxe et al., 2014; Hu et al., 2020). Firstly, we analyse the waveforms of a given sta-
 145 tion using a CNN. This CNN processes the three-component waveform (comprising N_t
 146 time samples) and extracts a set of N_f features. The geographic location (latitude/longitude)

147 of the seismic station is then appended to produce a feature vector of size N_f+2 . This
 148 feature vector serves as an input for the second component: an MLP that recombines
 149 the time-series features and station location into a final station-specific feature vector
 150 of size N_q . This process is repeated for all N_s stations in the network using the same CNN
 151 and MLP components (i.e. the exact same operations are applied to each station indi-
 152 vidually). The convolution operations are performed only along the time axis. The out-
 153 put of the CNN after concatenation with each station location is then of size $N_s \times (N_f + 2)$,
 154 and the output of the MLP is of size $N_s \times N_q$.

155 After processing of the node attributes (the waveforms and locations of each sta-
 156 tion), the output of the MLP is max reduced over all stations to yield a graph feature
 157 vector. Empirically we have found that a max reduce yields better results than averag-
 158 ing or summation. The extracted features carry no physical meaning, and the informa-
 159 tion content of the feature vectors adapts to the type of aggregation during training. Hence,
 160 the most suitable type of aggregation needs to be determined experimentally. Finally,
 161 the graph feature vector is fed into a second MLP to predict the graph attributes, be-
 162 ing the latitude, longitude, depth, and magnitude of the seismic source. Each of these
 163 source attributes is scaled so that they fall within the continuous range of $-1 < x <$
 164 $+1$, enforced by a tanh activation function in the last layer in the network. In contrast
 165 to previous work (Perol et al., 2018; Lomax et al., 2019), no binning of the source char-
 166 acteristics is performed. Moreover, we do not perform event detection, as this has already
 167 been done in numerous previous studies (Dysart & Pulli, 1990; Li et al., 2018; Mousavi
 168 et al., 2019; Wu et al., 2019, and others) and is essentially a solved problem. Instead,
 169 we focus on the characterisation of a given seismic event. Note that the procedure above
 170 is intrinsically invariant to the number and ordering of the seismic stations: the feature
 171 extraction and re-combination with the geographic location is performed for each node
 172 individually and does not incorporate information from the other stations in the network.
 173 The aggregation and the resulting graph feature vector are also independent of the num-
 174 ber and ordering of stations. Finally, the seismic source characteristics are predicted from
 175 this invariant graph feature vector, and are hence completely independent of the network
 176 input ordering and size.

177 To regularise the learning process, we include dropout regularisation (Srivastava
 178 et al., 2014) with a dropout rate of 15 % between each layer in each model component.
 179 Since the mechanics of convolutional layers are different from “dense” layers (those defin-

180 ing the MLPs), we use *spatial dropout* regularisation (Tompson et al., 2015) that ran-
 181 domly sets entire feature maps of a convolutional layer to zero (as opposed to individ-
 182 ual elements in the feature maps). The use of dropout regularisation is dually motivated:
 183 first of all it reduces overfitting on the training set, as the model cannot rely on a sin-
 184 gle layer output (which could be randomly set to zero), promoting redundancy and gen-
 185 eralisation within the model. Secondly, by randomly perturbing the data flow within the
 186 neural networks, the model output becomes probabilistic. The probability distribution
 187 of the model predictions for a given event can be acquired by evaluating a given input
 188 multiple times at inference time, with the variability produced by the dropout regular-
 189 isation. This technique is commonly referred to as Bayesian dropout (Gal & Ghahra-
 190 mani, 2016), as it yields a posterior distribution and hence provides a means to estimate
 191 the epistemic uncertainty for the predictions.

192 **2.3 Data description and training procedure**

193 To construct a training set, we use ObsPy (Beyreuther et al., 2010) to download
 194 the broadband station inventory and earthquake catalogue of the Southern California
 195 Seismic Network (SCSN; Hutton et al., 2010) over the period 2000-2015. For both the
 196 seismic station and event locations, we limit the latitude range from 32° to 36° , and the
 197 longitude range from -120° to -116° . The lower earthquake magnitude limit is set to
 198 3 with no depth cut-off. In total, 1377 events and 187 stations are included in the data
 199 set. After downloading the three-component waveforms and removing the instrument
 200 response, we filter the waveforms to a 0.1-8 Hz bandpass and interpolate onto a common
 201 time base of $1 \leq t \leq 101$ seconds after the event origin time, over 2048 evenly spaced
 202 time samples (≈ 20 Hz sampling frequency). For an average P-wave speed of 6 km s^{-1} ,
 203 this time interval allows the stations at the far ends of the domain (roughly 440×440
 204 km in size) to record the event while keeping the data volume compact. The lower limit
 205 of the frequency band is chosen below the corner frequency of the earthquakes in this
 206 analysis ($M_w < 6$, with corresponding corner frequency $f_c > 0.2$ Hz; Madariaga, 1976)
 207 such that information regarding the seismic moment is retained. The upper frequency
 208 limit acknowledges the common notion that attenuation and scattering rapidly reduce
 209 the signal spectrum at higher frequencies. Although the start time of all selected wave-
 210 forms is fixed relative to their event origin time, the shift-equivariance of the convolu-
 211 tion layers ensures that the extracted features are not sensitive to their timing with re-

212 spect to the origin. Subsequent aggregation over the time-axis renders the features strictly
213 time-invariant. As a result, selecting a different start of the data time window (which
214 is inevitable when the event origin time is unknown) does not affect the model perfor-
215 mance. The processed waveforms are then scaled by their standard deviation and stored
216 in a database which includes the locations of the seismic stations that have recorded the
217 events. Note that not all stations are operational at the time of a given event, and hence
218 the number of stations with recordings of the event varies.

219 After processing the waveforms, the locations of the stations and seismic source are
220 scaled by the minimum and maximum latitude/longitude, so that the re-scaled locations
221 fall in the range of ± 1 . Such normalisation is generally considered good practice in deep
222 learning. Similarly, the source depth is scaled to fall in the same range by taking a min-
223 imum and maximum source depth of 0 and 30 km respectively. The earthquake magni-
224 tude is scaled taking a minimum and maximum of 3 and 6. The full data set is then ran-
225 domly split 80-20 into a training set and a validation set, respectively. A batch of train-
226 ing samples is generated on the fly between training epochs by randomly selecting 16 train-
227 ing events, and 50 randomly selected stations associated with each event, which we con-
228 sider to strike a good balance between data volume and memory consumption. When
229 a given event was recorded by fewer than 50 stations, the absent recordings are replaced
230 by zeros (which do not contribute to the model performance). The model performance
231 is evaluated through a mean absolute error loss between the predicted and target seis-
232 mic source characteristics (scaled between ± 1), and training is performed by minimisa-
233 tion of the loss using the ADAM algorithm (Kingma & Ba, 2017). Training is contin-
234 ued for 500 epochs, at which point the model performance has saturated. On a single
235 nVidia Tesla K80, the training phase took about 1 hour in total. Once trained, evalu-
236 ation of 1377 events with up to 50 stations each takes less than 5 s of computation time
237 (including data transfer overhead), or 3.5 ms per event.

238 **3 Results and Discussion**

239 **3.1 Reference model performance**

240 We evaluate the performance of the trained model on both the training and val-
241 idation data sets separately (Fig. 2a-e and Supplementary Figure S2). The model pos-
242 terior is estimated by maintaining dropout regularisation at inference time (as discussed

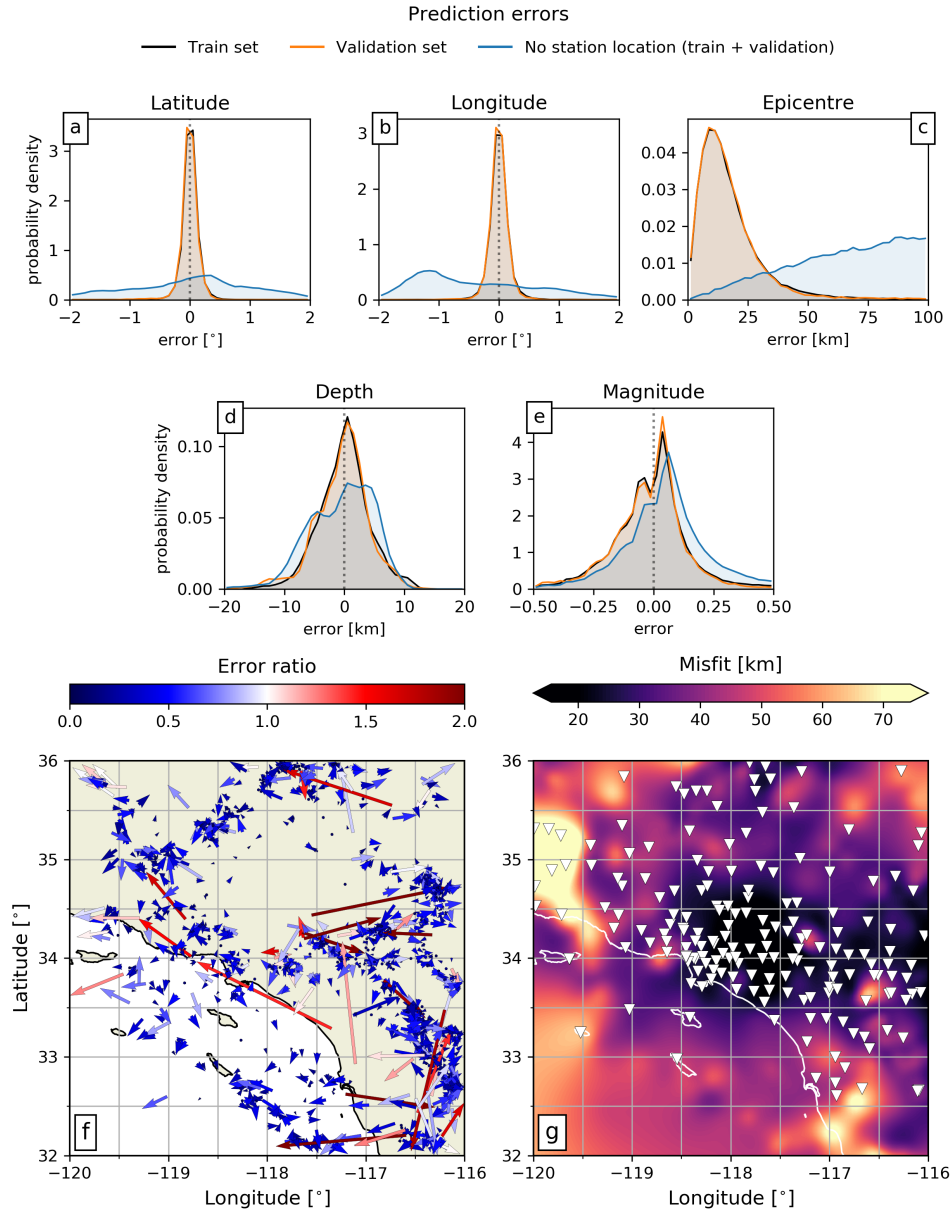


Figure 2. (a)-(e) Prediction error distributions for the trained model, for (a) latitude, (b) longitude, (c) epicentre, (d) depth, and (e) magnitude of each event. The model performance when including the station geographic locations is evaluated separately for the train and validation data sets, showing minimal overfitting. When the station locations are omitted, the performance is evaluated on the combined data set; (f) Residuals of the epicentral locations. Each arrow represents one catalogued event, starting at the predicted epicentre and pointing towards the catalogue epicentre. The colours indicate the ratio of the misfit over the 95 % confidence interval of the model posterior. Hence, blue colours indicate that the catalogue epicentre falls within the 95 % confidence interval, and red colours that the epicentre falls outside of it; (g) Overlay of the locations of seismic stations on the interpolated prediction error (in km)

243 in the previous section), and performing the inference 100 times on each event in the train-
244 ing and validation catalogues and calculating the corresponding mean and standard de-
245 viation. Overall, the performance is similar for either data set, which indicates that over-
246 fitting on the training set is minimal. The mean absolute difference between the cata-
247 logue values and the model predictions is less than 0.11° (≈ 13 km in distance) for the
248 latitude and longitude (which amounts to a mean epicentral location error of 18 km), 3.3 km
249 for the depth, and 0.13 for the event magnitude. While these predictions are not as pre-
250 cise as typical non-relocated estimates for Southern California (Powers & Jordan, 2010),
251 they are obtained without phase picking or waveform amplitude modelling, nor is a crustal
252 velocity models explicitly provided (though it is implicitly encoded in the catalogue hypocen-
253 tre locations). Hence, the method provides a reasonable first-order estimate of location
254 and magnitude that can serve as a starting point for subsequent refinement based on tra-
255 ditional seismological tools.

256 Since we can compute the posterior distribution for each event, we can compare
257 the confidence intervals given by the posterior with the true epicentre location error. In
258 Fig. 2f, we plot the residual vectors between the predicted epicentre locations and those
259 in the catalogue. To visualise the model uncertainty, we compute an error ratio metric
260 as the distance between the predicted and catalogued epicentres, normalised by the 95 %
261 confidence interval obtained from the model posterior. Hence, values less than 1 indi-
262 cate that the true epicentre location falls within the 95 % confidence interval, while val-
263 ues greater than 1 indicate the converse. Most of the predictions have an error ratio $<$
264 1. This assessment of the uncertainty in the predictions only addresses epistemic uncer-
265 tainties, but does not immediately address aleatoric uncertainties (errors or bias on the
266 SCSN catalogue). The epicentral errors reported for the SCSN catalogue are approxi-
267 mately 2 km, even though an in-depth analysis of these errors suggests that this error
268 assessment is somewhat over-estimated (Powers & Jordan, 2010). The expected aleatoric
269 uncertainties are therefore much smaller than the epistemic uncertainties given by the
270 model posterior distribution.

271 The spatially interpolated prediction error seems partly correlated with the local
272 density of seismic stations (Fig. 2g), as regions with the highest station density also ex-
273 hibit a low prediction error. The largest systematic errors are found in the northwest and
274 southeast corners of the selected domain, where the station density is low and where the
275 model seems unable to achieve the bounding values of latitude and longitude. This ob-

276 servation can be explained by the behaviour of the tanh activation function, which asymp-
277 totically approaches its range of ± 1 , corresponding with the range of latitudes and lon-
278 gitudes of the training samples. Hence, increasingly larger activations are required to push
279 the final location predictions towards the boundaries of the domain, biasing the results
280 towards the interior. This highlights a fundamental trade-off between resolution (pre-
281 diction accuracy) in the interior of the data domain, and the maximum amplitude of the
282 predictions (which also applies to linear activation functions).

283 Lastly, we perform additional analyses of the sensitivity of the predictions to the
284 signal-to-noise ratio, waveform pre-processing, and epicentre location (Supplementary
285 Figures S4-S6). These analyses show that the predictions are rather robust to the event
286 magnitude (as a proxy for signal-to-noise ratio), and insensitive to instrument correc-
287 tions. Moreover, preliminary tests, in which we adopted a filter passband of 0.5-5 Hz,
288 indicated that the choice for the pre-filtering frequency band had little influence on the
289 model performance. When the model is provided with waveforms belonging to an event
290 with an epicentre outside of the selected training domain, the model predictions for the
291 epicentre location collapse to an average value around the centre of the domain (Sup-
292 plementary Figure S6). Fortunately, the uncertainty of the predictions (inferred from the
293 posterior distribution of each event) is also much larger than for events that are located
294 within the domain. Thus, exterior events can be distinguished from interior events through
295 the inferred precision.

296 **3.2 Influence of geographic information on location accuracy**

297 A direct test to assess whether the station geographic location information is ac-
298 tually used in making the predictions (and therefore holds predictive value), we perform
299 inference on the full data set, but set the station coordinates to a fixed mean value of
300 $(34^\circ, -118^\circ)$ – see Fig. 2a-e and Supplementary Figure S3. While the predictions for the
301 event magnitude remain mostly unchanged, the estimation of the epicentre location de-
302 teriorates and becomes broadly distributed (typical for random predictions). This clearly
303 indicates that the station location information plays an important role in estimating the
304 epicentre locations. Thus, the adopted GNN approach, in which station location infor-
305 mation is provided explicitly, holds an advantage over station-location agnostic meth-
306 ods. Interestingly, the event magnitude is almost as well resolved as when the station
307 coordinates are included, which suggests that the model relies on the waveform data but

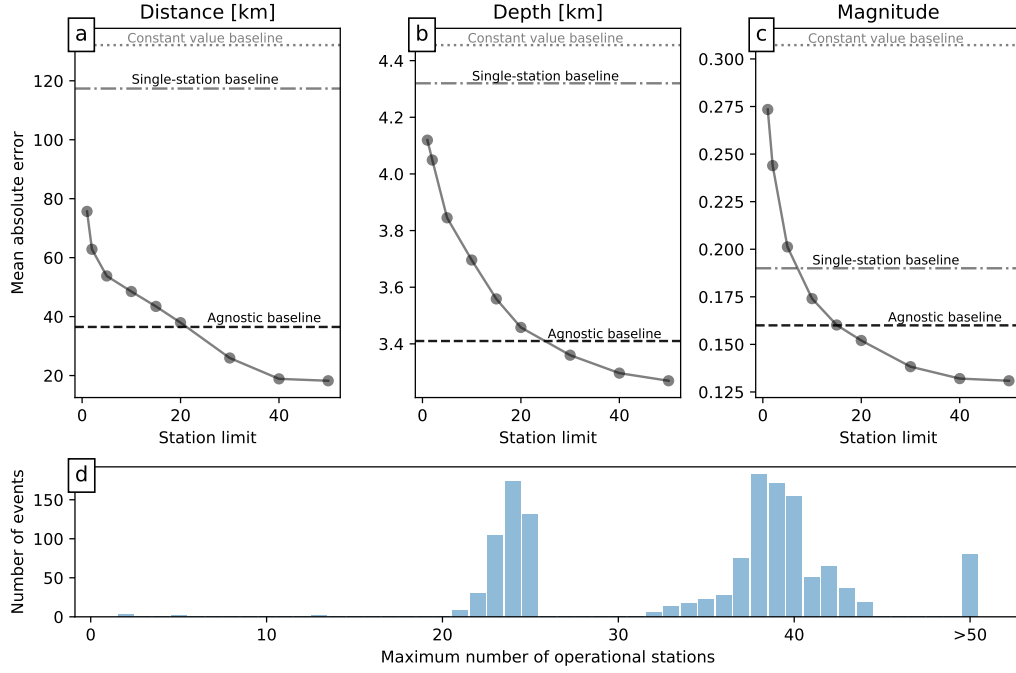


Figure 3. Effect of the number of available stations on the mean absolute error of the model predictions for (a) epicentral location, (b) hypocentral depth, and (c) event magnitude. When the number of stations included at inference time is increased, the misfit between the model predictions and the catalogue values decreases. The horizontal dashed and/or dotted lines in the top panels represents the baselines discussed in the text. Panel (d) displays the frequency distribution of the number of stations recording a given event.

308 not on station locations to estimate the magnitude. This was also observed by Mousavi
 309 & Beroza (2020b), who proposed that the relative timing of the P- and S-wave arrivals
 310 may encode epicentral distance information. Combined with the amplitude of the wave-
 311 forms, this may implicitly encode magnitude information.

312 Related to this, we investigate the effect of the (maximum) number of stations in-
 313 cluded at inference time by selecting, for each event, the stations recording the waveforms
 314 with the M highest standard deviations. All other waveforms are set to zero and there-
 315 fore do not contribute to the predictions. If a given event was recorded by fewer than
 316 M stations, only the maximum number of operational stations was used with no aug-
 317 mentation. We perform the inference for $M = \{1, 2, 5, 10, 15, 20, 30, 40, 50\}$ stations, and
 318 compute the mean absolute error of the predictions for the epicentre location (expressed

319 as a distance in km; Fig. 3a), hypocentral depth (Fig. 3b), and event magnitude (Fig. 3c).
 320 For all the predicted quantities, we observe that the misfit with the catalogue values rapidly
 321 decreases with the maximum number of stations included in the analysis, until the per-
 322 formance saturates at around $M \geq 40$. The reason for this saturation may lie in the
 323 distribution of the number of operational stations per event (Fig. 3d). Since the major-
 324 ity of catalogued events is recorded by fewer than 40 stations, increasing M beyond 40
 325 is only potentially beneficial only for a small number of events. For reference, we com-
 326 pute two performance baselines: firstly, we take the mean value of each quantity (lat-
 327 itude, longitude, depth, magnitude) over the catalogue and calculate the mean absolute
 328 error relative to these. This baseline represents the performance of a “biased coin flip”
 329 (i.e. random guessing). Secondly, we train our model specifically using only a single sta-
 330 tion per training sample, through which the method specialises to single-waveform anal-
 331 ysis (c.f. Perol et al., 2018; Lomax et al., 2019; Mousavi & Beroza, 2020b). These base-
 332 lines are included in Fig. 3 as horizontal dotted and dashed-dotted lines for the mean
 333 absolute error relative to the (constant value) mean, and for the single-station model,
 334 respectively. Strikingly, the model that was trained on the single-station waveforms achieves
 335 worse performance in terms of the predicted hypocentre locations than the model trained
 336 on 50 stations, but using only a single station at inference time. A possible explanation
 337 for this, is that the single-station model may have gotten attracted to a poor local min-
 338 imum in the loss landscape, after which the model started over-fitting, whereas the 50-
 339 station model was able to generalise better and descended into a better local minimum.

340 Lastly, we compare our model performance with a model that treats the seismic
 341 network as an Euclidean object, and hence has no explicit knowledge of the geographic
 342 locations of the seismic stations (“station-location agnostic”). This station-location ag-
 343 nostic model only features components #1 and #3 (see Fig. 1 and Supplementary Text
 344 S3 for details) and does not incorporate the station locations among the data features.
 345 Instead, the stations appear in a fixed order in a matrix of size $N_s \times N_t \times 3$, where $N_s =$
 346 256 denotes the total number of stations in the network (187) plus zero padding to make
 347 N_s an integer power of two. Potentially, the station-location agnostic model is able to
 348 “learn” the configuration of the seismic network and implicitly utilise station locations
 349 in predicting the seismic source characteristics. As in most traditional CNN approaches,
 350 we use a 2D kernel of size $k_s \times k_t$ with $k_s = 3$ so that information from “neighbour-
 351 ing” stations (i.e. sequentially appearing in the grid, which does not imply geographic

352 proximity) is combined into the next layer of the model. Downsampling of the data is
353 performed along both the temporal and station axes. Even though the number of free
354 parameters of the station-location agnostic model is almost twice that of the graph-based
355 model (owing to the larger convolutional kernels), and even though the model has ac-
356 cess to all the stations simultaneously, the prediction error of the seismic source param-
357 eters is significantly larger (dashed line in Fig. 3). Moreover, the station-location agnos-
358 tic model required 5 times more computation time per training epoch. Hence, the GNN
359 approach proposed here offers substantial benefits in terms of predictive power and ease
360 of training.

361 **3.3 Potential applications**

362 The method proposed in this study does not require the intervention of an analyst
363 to prepare or verify the model input data (e.g. picking P- and S-wave first arrivals), and
364 so it can operate autonomously. This, combined with the rapid inference time of ≈ 3.5 ms
365 for 50 stations, opens up applications in automated source characterisation that require
366 a rapid response, such as earthquake early warning (EEW; Allen & Melgar, 2019), emer-
367 gency response, and timely public dissemination. The aim of this study is to demonstrate
368 the potential of incorporating seismic station locations (and possibly other node or edge
369 attributes in a graph structure). Therefore, the model architecture was not optimised
370 with the purpose of EEW in mind. Nonetheless, its modular nature allows for modifi-
371 cations required to accommodate the real-time demands of EEW.

372 The first out of three components of this model consists of a CNN that analyses
373 the waveforms of each seismic station and yields a set of station-specific features. The
374 advantage of using a CNN is that it has immediate access to all the available informa-
375 tion to produce a set of features optimal for the subsequent MLP components. Alter-
376 natively, a different class of deep neural networks suitable for time-series analysis, the
377 Recurrent Neural Networks (RNN; Hochreiter & Schmidhuber, 1997; Sherstinsky, 2020),
378 allows for online (real-time) processing of time series. Within the generalised framework
379 of GNNs (Battaglia et al., 2018), replacing the first CNN component with an RNN pro-
380 duces an equally valid model architecture, still independent of the number and order-
381 ing of stations. As such, for each new data entry the model updates its prediction, tak-
382 ing into account previously seen data (the “memory” of the RNN). A robust prediction
383 will be one for which the output of the model converges to a stable estimate of hypocen-

384 tre location and magnitude. Since we here employed a CNN rather than an RNN, we
385 do not know how much time since the first ground motions is required to converge to a
386 stable prediction, and we anticipate that this convergence depends on the quality and
387 consistency of the data. Moreover, different components of the prediction may converge
388 at different rates: while the hypocentre estimate may be governed by the (first) arrival
389 of seismic energy at the various stations in the region (and therefore on the station den-
390 sity), the magnitude estimate is potentially controlled by the duration of the moment-
391 rate function (Meier et al., 2017). Owing to the opacity of our deep learning method,
392 we cannot directly assess which part of the input governs which part in the output, and
393 so this will need to be assessed empirically.

394 As mentioned in Section. 2.2, we focussed our efforts on seismic source character-
395 isation and not event detection. For any EEW task, earthquake detection is a crucial first
396 step, which fortunately has been demonstrated to be a task suitable for machine learn-
397 ing methods (e.g. Dysart & Pulli, 1990; Li et al., 2018; Mousavi et al., 2019; Wu et al.,
398 2019). In the methods proposed in the present study, earthquake detection could be per-
399 formed by adding an additional graph attribute (alongside latitude, longitude, depth,
400 and magnitude) indicating whether or not an event has been detected (similar to Perol
401 et al., 2018; Lomax et al., 2019). Alternatively, a dedicated detection algorithm (based
402 on machine learning or otherwise), could run in parallel and trigger the source charac-
403 terisation algorithm once an event has been detected. This second approach significantly
404 reduces computational overhead. Flexibility in the number of stations included in the
405 model input facilitates processing of an expanding data set as more seismic stations ex-
406 perience ground shaking after the first detection.

407 For the applications of emergency response and information dissemination, the real-
408 time requirements are less stringent, so that some response time may be sacrificed in favour
409 of prediction accuracy, maintaining the CNN component #1. Our method can be read-
410 ily applied to automated earthquake catalogue generation in regions where large volumes
411 of raw data exist, but which have not been fully processed. This typically arises in af-
412 tershock campaigns with stations that were not telemetered, for instance Ocean Bottom
413 Seismometers. Given the relatively small size of the GNN employed here, re-training a
414 pre-trained model on data from a different region is relatively inexpensive. Out of the
415 110,836 trainable parameters, less than half (42,244) reside in the second and third com-
416 ponents of the network. The first CNN component is completely agnostic to any spa-

417 tial or regional information, as it only extracts features from time series of individual sta-
418 tions. Hence, if the waveforms in the target region are similar to those in the initial train-
419 ing region, the first component requires no re-training. This leaves only the smaller sec-
420 ond and third MLP components to be re-trained and adapted to the characteristics of
421 the target region. As such, fewer training seismic events than employed for the initial
422 training will be required for fine-tuning of the model. It is crucial to realise here that
423 the second and third components potentially encode the crustal velocity structure and
424 local site amplifications, and are therefore specific to the domain that was selected dur-
425 ing training (Southern California). Direct application of the trained model to other re-
426 gions without retraining is unwarranted. The scaling of the re-trained model performance
427 with the number of stations will need to be assessed empirically, as it may be sensitive
428 to station redundancy, and spatial coverage and density.

429 Aside from automatically providing an earthquake catalogue, the estimates of the
430 seismic source locations can offer a suitable starting point for additional seismological
431 analyses. With the re-trained model, the predicted hypocentre locations yield approx-
432 imate phase arrival times at the various stations in the seismic network, which serve as
433 a basis to set the windows for cross-correlation time-delay estimation and subsequent double-
434 difference relocation. Grid-search based inversion efforts could be directed to a region
435 around the predicted hypocentre location, rather than expanding the search of candi-
436 date source locations to a much larger (regional) domain. Even though the model pre-
437 dictions for the epicentral locations are larger than what conventional seismological tech-
438 niques can achieve, there is merit in deep-learning based automated source character-
439 isation to expedite current seismological workflows.

440 Lastly, we point out that the GNN-approach is rather general, and that it may be
441 adopted in other applications such as seismic event detection or classification, that ben-
442 efit from geographic or relational information of the seismic network. Aside from pre-
443 dicting "global" graph attributes, like was done in this study, GNNs can also be employed
444 to predict node or edge attributes. Examples of such attributes include site amplifica-
445 tion factors and event detections for the nodes (seismic stations), and phase associations
446 for the edges. Since many geophysical data are inherently non-Euclidean, graph-based
447 approaches offer a natural choice for the analysis of these data, and permit creative so-
448 lutions to present-day challenges.

449 4 Conclusions

450 In this study we propose a method to incorporate the geometry of a seismic net-
451 work into deep learning architectures using a Graph Neural Network (GNN) approach,
452 applied to the task of seismic source characterisation (earthquake location and magni-
453 tude estimation). By incorporating the geographic location of stations into the learn-
454 ing and prediction process, we find that the deep learning model achieves superior per-
455 formance in predicting the seismic source characteristics (epicentral latitude/longitude,
456 hypocentral depth, and event magnitude) compared to a model that is agnostic to the
457 layout of the seismic network. In this way, multi-station waveforms can be incorporated
458 while preserving flexibility to the number of available seismic stations, and invariance
459 to the ordering of the station recordings. The GNN-based approach warrants the explo-
460 ration of new avenues in earthquake early warning and rapid earthquake information dis-
461 semination, as well as in automated earthquake catalogue generation or other seismo-
462 logical tasks.

463 Acknowledgements

464 Acknowledgments

465 We thank the Associate Editor and two anonymous reviewers for their thoughtful com-
466 ments on the manuscript. MvdE is supported by French government through the UCA^{JEDI}
467 Investments in the Future project managed by the National Research Agency (ANR) with
468 the reference number ANR-15-IDEX-01. The authors acknowledge computational resources
469 provided by the ANR JCJC E-POST project (ANR-14-CE03-0002-01JCJC E-POST).
470 Python codes and the pre-trained model are available from: <https://doi.org/10.6084/m9.figshare.12231077>
471

472 **References**

- 473 Allen, R. M., & Melgar, D. (2019). Earthquake Early Warning: Advances, Scientific
474 Challenges, and Societal Needs. *Annual Review of Earth and Planetary Sciences*,
475 47(1), 361–388. doi: 10.1146/annurev-earth-053018-060457
- 476 Battaglia, P. W., Hamrick, J. B., Bapst, V., Sanchez-Gonzalez, A., Zambaldi, V.,
477 Malinowski, M., . . . Pascanu, R. (2018, October). Relational inductive biases,
478 deep learning, and graph networks. *arXiv:1806.01261 [cs, stat]*.
- 479 Beyreuther, M., Barsch, R., Krischer, L., Megies, T., Behr, Y., & Wassermann, J.
480 (2010, May). ObsPy: A Python Toolbox for Seismology. *Seismological Research*
481 *Letters*, 81(3), 530–533. doi: 10.1785/gssrl.81.3.530
- 482 Bronstein, M. M., Bruna, J., LeCun, Y., Szlam, A., & Vandergheynst, P. (2017,
483 July). Geometric Deep Learning: Going beyond Euclidean data. *IEEE Signal*
484 *Processing Magazine*, 34(4), 18–42. doi: 10.1109/MSP.2017.2693418
- 485 Cui, Z., Henrickson, K., Ke, R., & Wang, Y. (2019). Traffic Graph Convolutional
486 Recurrent Neural Network: A Deep Learning Framework for Network-Scale Traf-
487 fic Learning and Forecasting. *IEEE Transactions on Intelligent Transportation*
488 *Systems*, 1–12. doi: 10.1109/TITS.2019.2950416
- 489 Duvenaud, D. K., Maclaurin, D., Iparraguirre, J., Bombarell, R., Hirzel, T., Aspuru-
490 Guzik, A., & Adams, R. P. (2015). Convolutional Networks on Graphs for
491 Learning Molecular Fingerprints. In C. Cortes, N. D. Lawrence, D. D. Lee,
492 M. Sugiyama, & R. Garnett (Eds.), *Advances in Neural Information Processing*
493 *Systems 28* (pp. 2224–2232). Curran Associates, Inc.
- 494 Dysart, P. S., & Pulli, J. J. (1990, December). Regional seismic event classification
495 at the NORESS array: Seismological measurements and the use of trained neural
496 networks. *Bulletin of the Seismological Society of America*, 80(6B), 1910–1933.
- 497 Fukushima, K. (1980, April). Neocognitron: A self-organizing neural network model
498 for a mechanism of pattern recognition unaffected by shift in position. *Biological*
499 *Cybernetics*, 36(4), 193–202. doi: 10.1007/BF00344251
- 500 Gal, Y., & Ghahramani, Z. (2016). Dropout as a Bayesian Approximation: Repre-
501 senting Model Uncertainty in Deep Learning. *Proceedings of the 33rd International*
502 *Conference on International Conference on Machine Learning*, 48, 1050–1059.
- 503 Gilmer, J., Schoenholz, S. S., Riley, P. F., Vinyals, O., & Dahl, G. E. (2017, June).
504 Neural Message Passing for Quantum Chemistry. *Proceedings of the 34th Interna-*

- 505 *tional Conference on Machine Learning*, 70, 1263–1272.
- 506 Gori, M., Monfardini, G., & Scarselli, F. (2005, July). A new model for learn-
507 ing in graph domains. In *Proceedings. 2005 IEEE International Joint Con-*
508 *ference on Neural Networks, 2005*. (Vol. 2, p. 729-734 vol. 2). doi: 10.1109/
509 IJCNN.2005.1555942
- 510 Hamilton, W. L., Ying, R., & Leskovec, J. (2017, December). Inductive representa-
511 tion learning on large graphs. In *Proceedings of the 31st International Conference*
512 *on Neural Information Processing Systems* (pp. 1025–1035). Long Beach, Califor-
513 nia, USA: Curran Associates Inc.
- 514 Hochreiter, S., & Schmidhuber, J. (1997, November). *Long Short-Term Memory*.
515 MIT Press.
- 516 Hu, W., Xiao, L., & Pennington, J. (2020, January). Provable Benefit of Orthogonal
517 Initialization in Optimizing Deep Linear Networks. *arXiv:2001.05992 [cs, math,*
518 *stat]*.
- 519 Hutton, K., Woessner, J., & Hauksson, E. (2010, April). Earthquake Monitoring in
520 Southern California for Seventy-Seven Years (1932–2008). *Bulletin of the Seismo-*
521 *logical Society of America*, 100(2), 423–446. doi: 10.1785/0120090130
- 522 Käußl, P., Valentine, A. P., O’Toole, T. B., & Trampert, J. (2014, March). A frame-
523 work for fast probabilistic centroid-moment-tensor determination—inversion of
524 regional static displacement measurements. *Geophysical Journal International*,
525 196(3), 1676–1693. doi: 10.1093/gji/ggt473
- 526 Kingma, D. P., & Ba, J. (2017, January). Adam: A Method for Stochastic Opti-
527 mization. *arXiv:1412.6980 [cs]*.
- 528 Kriegerowski, M., Petersen, G. M., Vasyura-Bathke, H., & Ohrnberger, M. (2019,
529 March). A Deep Convolutional Neural Network for Localization of Clustered
530 Earthquakes Based on Multistation Full Waveforms. *Seismological Research Let-*
531 *ters*, 90(2A), 510–516. doi: 10.1785/0220180320
- 532 LeCun, Y., Bengio, Y., & Hinton, G. (2015, May). Deep learning. *Nature*,
533 521(7553), 436–444. doi: 10.1038/nature14539
- 534 Li, Z., Meier, M.-A., Hauksson, E., Zhan, Z., & Andrews, J. (2018). Machine Learn-
535 ing Seismic Wave Discrimination: Application to Earthquake Early Warning. *Geo-*
536 *physical Research Letters*, 45(10), 4773–4779. doi: 10.1029/2018GL077870
- 537 Lomax, A., Michelini, A., & Jozinović, D. (2019, March). An Investigation of Rapid

- 538 Earthquake Characterization Using Single-Station Waveforms and a Convolu-
539 tional Neural Network. *Seismological Research Letters*, 90(2A), 517–529. doi:
540 10.1785/0220180311
- 541 Madariaga, R. (1976). Dynamics of an expanding circular fault. *Bull. Seismol. Soc.*
542 *Am*, 639–666.
- 543 Meier, M.-A., Ampuero, J. P., & Heaton, T. H. (2017, September). The hidden sim-
544 plicity of subduction megathrust earthquakes. *Science*, 357(6357), 1277–1281. doi:
545 10.1126/science.aan5643
- 546 Monti, F., Boscaini, D., Masci, J., Rodolà, E., Svoboda, J., & Bronstein, M. M.
547 (2017, July). Geometric Deep Learning on Graphs and Manifolds Using Mix-
548 ture Model CNNs. In *2017 IEEE Conference on Computer Vision and Pattern*
549 *Recognition (CVPR)* (pp. 5425–5434). doi: 10.1109/CVPR.2017.576
- 550 Mousavi, S. M., & Beroza, G. C. (2020a). Bayesian-Deep-Learning Estimation of
551 Earthquake Location From Single-Station Observations. *IEEE Transactions on*
552 *Geoscience and Remote Sensing*, 1–14. doi: 10.1109/TGRS.2020.2988770
- 553 Mousavi, S. M., & Beroza, G. C. (2020b). A Machine-Learning Approach for
554 Earthquake Magnitude Estimation. *Geophysical Research Letters*, 47(1),
555 e2019GL085976. doi: 10.1029/2019GL085976
- 556 Mousavi, S. M., Zhu, W., Sheng, Y., & Beroza, G. C. (2019, July). CRED: A Deep
557 Residual Network of Convolutional and Recurrent Units for Earthquake Signal
558 Detection. *Scientific Reports*, 9(1), 1–14. doi: 10.1038/s41598-019-45748-1
- 559 Perol, T., Gharbi, M., & Denolle, M. (2018, February). Convolutional neural net-
560 work for earthquake detection and location. *Science Advances*, 4(2), e1700578.
561 doi: 10.1126/sciadv.1700578
- 562 Powers, P. M., & Jordan, T. H. (2010). Distribution of seismicity across strike-slip
563 faults in California. *Journal of Geophysical Research: Solid Earth*, 115(B5). doi:
564 10.1029/2008JB006234
- 565 Qi, C. R., Yi, L., Su, H., & Guibas, L. J. (2017, December). PointNet++: Deep
566 hierarchical feature learning on point sets in a metric space. In *Proceedings of*
567 *the 31st International Conference on Neural Information Processing Systems* (pp.
568 5105–5114). Long Beach, California, USA: Curran Associates Inc.
- 569 Rosenblatt, F. (1957). *The Perceptron: A Perceiving and Recognizing Automaton*
570 (Tech. Rep. No. 85-60-1). Buffalo, New York: Cornell Aeronautical Laboratory.

- 571 Rumelhart, D. E., Hinton, G. E., & Williams, R. J. (1986, October). Learning repre-
572 sentations by back-propagating errors. *Nature*, *323*(6088), 533–536. doi: 10.1038/
573 323533a0
- 574 Sanchez-Gonzalez, A., Bapst, V., Cranmer, K., & Battaglia, P. (2019, September).
575 Hamiltonian Graph Networks with ODE Integrators. *arXiv:1909.12790 [physics]*.
- 576 Saxe, A., McClelland, J. L., & Ganguli, S. (2014). Exact solutions to the nonlinear
577 dynamics of learning in deep linear neural networks. In *International Conference*
578 *on Learning Representations*.
- 579 Scarselli, F., Gori, M., Tsoi, A. C., Hagenbuchner, M., & Monfardini, G. (2009, Jan-
580 uary). The graph neural network model. *IEEE transactions on neural networks*,
581 *20*(1), 61–80. doi: 10.1109/TNN.2008.2005605
- 582 Schramowski, P., Stammer, W., Teso, S., Brugger, A., Luigs, H.-G., Mahlein, A.-K.,
583 & Kersting, K. (2020, January). Right for the Wrong Scientific Reasons: Revising
584 Deep Networks by Interacting with their Explanations. *arXiv:2001.05371 [cs,*
585 *stat]*.
- 586 Sherstinsky, A. (2020, March). Fundamentals of Recurrent Neural Network (RNN)
587 and Long Short-Term Memory (LSTM) network. *Physica D: Nonlinear Phenom-*
588 *ena*, *404*, 132306. doi: 10.1016/j.physd.2019.132306
- 589 Srivastava, N., Hinton, G., Krizhevsky, A., Sutskever, I., & Salakhutdinov, R.
590 (2014). Dropout: A simple way to prevent neural networks from overfitting.
591 *Journal of Machine Learning Research*, *15*(56), 1929–1958.
- 592 Tompson, J., Goroshin, R., Jain, A., LeCun, Y., & Bregler, C. (2015, June). Ef-
593 ficient object localization using Convolutional Networks. In *2015 IEEE Confer-*
594 *ence on Computer Vision and Pattern Recognition (CVPR)* (pp. 648–656). doi:
595 10.1109/CVPR.2015.7298664
- 596 Wang, Y., Sun, Y., Liu, Z., Sarma, S. E., Bronstein, M. M., & Solomon, J. M. (2019,
597 October). *Dynamic Graph CNN for Learning on Point Clouds*. Association for
598 Computing Machinery.
- 599 Wu, Y., Lin, Y., Zhou, Z., Bolton, D. C., Liu, J., & Johnson, P. (2019, January).
600 DeepDetect: A Cascaded Region-Based Densely Connected Network for Seismic
601 Event Detection. *IEEE Transactions on Geoscience and Remote Sensing*, *57*(1),
602 62–75. doi: 10.1109/TGRS.2018.2852302
- 603 Zhou, J., Cui, G., Zhang, Z., Yang, C., Liu, Z., Wang, L., . . . Sun, M. (2019,

604 July). Graph Neural Networks: A Review of Methods and Applications.
605 *arXiv:1812.08434 [cs, stat]*.